Microindentation of Aluminum

FUQIAN YANG, LINGLING PENG, and KENJI OKAZAKI

A simple model was developed to correlate the plastic energy dissipated in microindentation to the applied load and the average dislocation density underneath the indentation. The model predicted that the plastic energy dissipated in a loading-unloading cycle was proportional to the 3/2 power of the indentation load as well as to the 3/4 power of the average dislocation density underneath the indentation. The experimental results from the microindentation tests of the annealed Al and the equal channel angular extrusion (ECAE)–deformed Al supported the proposed model. A variation of the microhardness to the various sections of the ECAE-deformed Al was observed, suggesting that the Al rod was deformed to varying degrees of plastic deformation after only a single ECAE pass. The hardness of the most severely deformed sample showed the highest hardness, and the annealed sample showed the lowest hardness. Also, plastic recovery was observed in the indentation of the ECAE-deformed Al, which suggested a kind of Bauschinger effect took place.

I. INTRODUCTION

IN the last decades, there has been considerable interest in severe plastic deformation (SPD) that can achieve grain size refinement in metallic alloys. The highly deformed materials appear to retain high levels of internal strain and high dislocation densities, and grain boundaries have been described as being in nonequilibrium state.[1] Such materials display unique features such as high strength with ductility, superplasticity at moderate temperatures, and high strain rates.

Of the existing SPD processes, equal channel angular extrusion (ECAE) and high pressure torsion (HPT) are the most versatile and potent processes for fabricating materials of ultrafine structure in a large quantity. In ECAE, a rod-shape sample is extruded repetitively through a die with equal channels.[2–6] In HPT, a thin disk is subjected to a high pressure and concurrent torsion straining.[7] It is, however, generally believed that the ECAE process can be scaled relatively easily to produce large bulk samples[8] and is amenable to simplification.

The ECAE process appears to be effective with aluminum alloys and makes it possible to produce equiaxed grains of submicrometer sizes that give superplastic ductility at elevated temperatures[9] and the as-extruded aluminum alloys can be formed into domes[10] or rolled into thin sheets without a significant loss in their superplastic properties.[11] In most cases, the microstructure has been described as "submicron polycrystals" with no specific analysis, and the mechanical behavior under static and dynamic loading has been evaluated mostly by using tensile and compression tests.[12–16] The understanding of the fundamental mechanisms controlling the mechanical deformation as well as the evolution of the microstructure, however, is still at a very early stage.

The microindentation is a very simple and convenient method for determining time-independent plastic flow in materials. An indenter is pushed onto the surface of a sample to evoke plastic flow in indentation test, both the load and the displacement of the indenter are recorded. Based on the load-displacement curve and the impression profile, the mechanical response of a material can be evaluated. The microhardness, H_V, being used to describe the plastic behavior of a material, is defined as the ratio of the indentation load to the contact area between the indenter and the sample. That is (for the Vickers indenter),

$$H_V = 2F \sin \phi / D^2 \qquad [1]$$

where F is the indentation load, ϕ is a half of the included angle between opposite faces of a pyramid (68 deg), and D is the diagonal length of the impression profile. Despite the advantage of the indentation technique as a method to characterize local material behavior, there is no systematic study on the characterization of local plastic deformation of the ECAE-deformed materials.

Generally, the hardness of a material measured by conventional techniques is a function of the stress state of the material. In 1932, Kokubo demonstrated the influence of applied bending stress on the measurement of the Vickers hardness in a variety of metals and alloys.[17] Since then, extensive studies have been conducted to further explore the phenomenon using unaxial and biaxial stress states and measuring the hardness by Brinell, Rockwell, and Vickers methods.[18–21] Up to now, most work considering the effect of applied stresses on the indentation of materials have focused on indentation deformation and the effect of applied stresses on the pileup of the indentation. However, the indentation deformation of the ECAE-deformed materials has not been addressed.

In this work, single pass extrusion of Al rod is performed at ambient temperature. The annealed Al rod is extruded only halfway through the die. Such an extrusion would produce a highly inhomogeneous microstructure, which allows us to evaluate the inhomogeneous deformation in the ECAE-deformed Al by obtaining samples from different locations of the deformed Al rod. The microhardness in the ECAE-deformed Al is evaluated in order to assess the effect of severe plastic deformation on the mechanical response and to determine the inhomogeneous deformation introduced in the ECAE process. Eventually, the plastic energy dissipated

FUQIAN YANG, Assistant Professor, LINGLING PENG, Postdoctoral Student, and KENJI OKAZAKI, Full Professor, are with the Department of Chemical and Materials Engineering, University of Kentucky, Lexington, KY 40506. Contact e-mail: fyang0@engr.uky.edu

Manuscript submitted March 19, 2004.

in indentations is correlated with the indentation load and dislocation density underneath the indentation.

II. INDENTATION MODEL

According to the dislocation theory, the relation between the shear stress and the effective dislocation density, ρ, can be expressed as[22,23]

$$\tau = \alpha MG\mathrm{b}\sqrt{\rho} \quad [2]$$

if the influence of dislocation density on the flow stress is dominant. Here, G is the shear modulus, b is the magnitude of the Burgers vector, and α is a constant (typically 0.2 to 0.4[22,24–28]). Ashby[29] split the difference in assuming $\alpha = 0.3$. The Taylor factor, M, can vary from 1 (pure shear) to about 3.67 for single crystals and is typically, in tension, 3.06 for polycrystals.[30] From the von Mises flow rule in the theory of continuum plasticity,[26] the relation between the uniaxial tensile stress and the shear stress is

$$\sigma = \sqrt{3}\tau \quad [3]$$

Using Eq. [3], one can write Eq. [2] as

$$\sigma = \sqrt{3}\alpha MG\mathrm{b}\rho^{1/2} \quad [4]$$

where σ is the tensile flow stress. The microhardness H as a representative of the plastic flow is related to the flow stress as[31,32]

$$H = 3\sigma \quad [5]$$

Substituting Eq. [4] into Eq. [5], one obtains the relation between the dislocation density and the microhardness as

$$H = 3\sqrt{3}\alpha MG\mathrm{b}\rho^{1/2} \quad [6]$$

Following the approach used by Hill[32,33,34] in simulating the indentation problem as the expansion of a spherical cavity, one can assume that the indentation pressure is transmitted *via* an incompressible hydrostatic core of a hemisphere having a radius, c, equal to the size of the plastic zone underneath the indenter. Decompose the normal stress on the surface of the hemisphere into the horizontal component perpendicular to the loading direction of the indentation and the vertical component parallel to the direction of the indentation, and take the integration of the vertical component over the surface of the hemisphere. Using the equilibrium equation in the direction of the indentation, one obtains

$$F = \frac{2}{3}\pi c^2\sigma \quad [7]$$

Substituting Eq. [6] into Eq. [7], the plastic zone developed in the indentation is found to be

$$c = \left(\frac{3F}{2\pi\sigma}\right)^{1/2} = \left(\frac{\sqrt{3}}{2\pi\alpha MG\mathbf{b}}\right)^{1/2} F^{1/2}\rho^{-1/4} \quad [8]$$

The size of the plastic zone increases with increasing the indentation load and decreases with increasing the dislocation density.

During the loading process, the total energy, E_{loading}, given to a specimen can be calculated as

$$E_{\text{loading}} = \int_0^{\delta_{\max}} F d\delta \quad [9]$$

where $\delta_{\max}$ is the maximum indentation depth at the maximum indentation load, $F_{\max}$. The energy is represented as the area under the loading curve. During the unloading process, elastic recovery occurs and the elastic energy released, $E_{\text{unloading}}$, is given by

$$E_{\text{unloading}} = \int_{\delta_r}^{\delta_{\max}} F d\delta \quad [10]$$

where δ_r is the residual indentation depth after totally removing the load. From Eqs. [9] and [10], the plastic energy dissipated in the specimen during the indentation is given by

$$E_{\text{plastic}} = E_{\text{loading}} - E_{\text{unloading}} = \int_0^{\delta_{\max}} F d\delta - \int_{\delta_r}^{\delta_{\max}} F d\delta \quad [11]$$

In general, the evolution of dislocation density can be better described by a change in dislocation density with respect to strain, which consists of two major terms: (1) the storage of dislocations and (2) the thermal recovery of immobile dislocations.[35] It has been demonstrated that annihilation mechanisms occur such that the effects of work hardening are minimized for the indentation of the ECAE-deformed Al.[36] Thus, it is reasonable to assume that the plastic strain developed in the ECAE-deformed Al during the indentation is proportional to the dislocation density.[23,29] Using Eq. [4], the plastic energy density dissipated in the specimen, $\Delta E_{\text{plastic}}$, can be related to the dislocation density as

$$\Delta E_{\text{plastic}} = \sigma \cdot \varepsilon = \beta \cdot \rho^{3/2} \quad [12]$$

where β is a constant. This plastic energy density increases with increasing the dislocation density with the 3/2 power.

For a Vickers indentation, the volume of the plastic zone, ΔV, can be calculated by the following equation[37] as

$$\Delta V = \sqrt{2}c^3\cot(\phi/3) \quad [13]$$

From Eqs. [12] and [13], the plastic energy dissipated, E_{plastic} (Eq. [11]), can be rewritten as

$$E_{\text{plastic}} = \int_0^{\Delta V} \Delta E_{\text{plastic}} \cdot dV \propto \Delta E_{\text{plastic}} \cdot \Delta V \propto F^{3/2}\rho^{3/4} \quad [14]$$

which is proportional to the 3/2 power of the indentation load, F, and the 3/4 power of the average dislocation density, ρ, underneath the indentation.

III. MATERIALS AND EXPERIMENTAL PROCEDURES

Pure (99 + pct) aluminum rods were purchased from Alfa Aesar, Ward Hill, MA. As-received rod (12 mm in diameter) was machined to a rod shape with diameter of 8 mm and length of 50.8 mm at ambient temperature. Prior to the ECAE process, machined Al rods were annealed at 773 K for 43.2 ks and furnace cooled to room temperature. The ECAE die consisted of two split blocks of tool steel (H-13), which were held together to form a single internal channel of circular equal cross section of diameter 8.0 mm with two channels meeting in an L-shape configuration. The angle between the two channels was 90 deg (Figure 1). The surface of the internal channel was lubricated with a lubricant (a mixture of

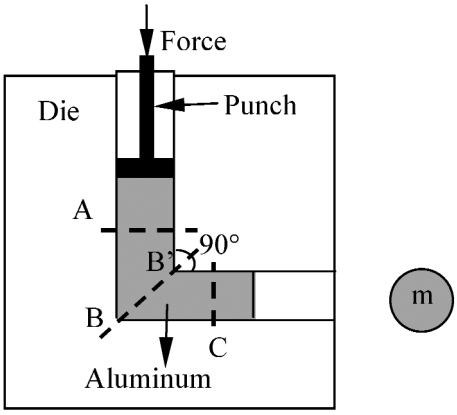

Fig. 1—Schematic diagram of the ECAE process.

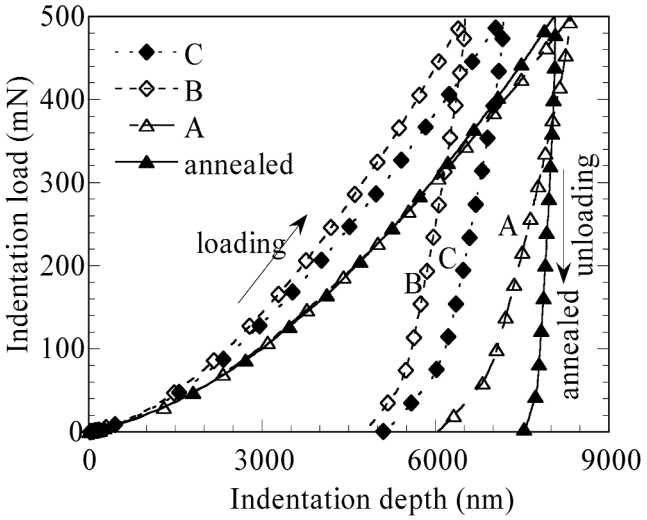

Fig. 2—Typical loading-unloading curves for the annealed and ECAE-deformed Al (Δ: sample A, ◇: sample B, ◆: sample C, and ▲: annealed sample).

MoS_2 powder and oil) to reduce the friction between the die wall and the Al rod. Single pass extrusion was performed at ambient temperature, and the annealed Al rod was extruded only halfway through the die, as shown in Figure 1. To determine the inhomogeneous deformation introduced in the ECAE process, specimens for indentation tests were cut from three different locations (A, B, and C; the distance between the cross section A and point B', as shown in Figure 1, was ~5 mm by using a water-cooled diamond saw. The specimens then were polished to obtain a smooth and mirrorlike surface. Severe plastic deformation was presented in samples B and C, which were extruded through the junction between two channels; and less plastic deformation was introduced in sample A, which only experienced simple extrusion.

Microindentation tests were performed by using a Vickers indenter on a microhardness tester (Micro Photonics, Irvine, CA). Indentations were made at the central position, *m,* for samples obtained from three different locations (A, B, and C in the ECAE-deformed Al), as shown in Figure 1, and also for annealed Al. Both the loading time and unloading time were 30 seconds without an intermediate pause. Prior to full indentation, a preload of 5 mN was applied to the indenter. Loading-unloading curves were recorded, from which the energy dissipated during a loading-unloading cycle was calculated by using Eq. [11]. Additionally, the diagonal lengths of an indentation mark were measured to calculate the Vickers hardness.

IV. RESULTS AND DISCUSSION

A. *Loading-Unloading Curves*

During the indentation test, the load applied to the indenter was increased at a constant loading rate to push it into the surface of a specimen and produced elastoplastic deformation. After reaching the predetermined maximum load, the load was immediately removed at a constant unloading rate, resulting in the recovery of the elastic portion. Figure 2 shows typical loading-unloading curves for the ECAE-deformed Al at three different sections of the rod, A, B, and C (Figure 1). For comparison, the corresponding loading-unloading curve for an annealed Al is also included. For a small indentation depth of less than 1 μm in the loading phase, the relations between the load and indentation depth (the displacement of the indenter) for all ECAE specimens are almost the same as that for the annealed. At deeper indentation depths, larger loads are required, especially for the ECAE specimens of B and C, and smaller loads for the specimen A and annealed Al. The results suggest that the indentation in the ECAE specimen B experiences the largest resistance. This is likely due to higher dislocation density in both samples B and C, as introduced in the ECAE, and the strong interaction between dislocations.

As shown in Figure 2, the slopes of the unloading curves for all three ECAE samples become less than that for the annealed Al. It is likely that this is due to the plastic recovery occurring in the unloading process. Due to pileup of dislocations and the strong interaction among dislocations, the mobile dislocations move back onto other slip planes under the back pressure during the unloading phase, which are combined and annihilated to lower the total strain energy. In other words, a kind of Bauschinger effect occurs in the ECAE sample during unloading.

For homogeneous materials, the relation between the indentation load and the maximum indentation depth can be described by the following equation:[38]

$$F = K_m \delta^n \qquad [15]$$

where K_m is a constant related to the elastoplastic behavior of the material and n is a constant exponent. Figure 3 shows the dependence of the maximum indentation load on the maximum indentation depth in a log-log plot. Here, a power index of 3/2 is observed for all the ECAE-processed and annealed Al, which is different from 2, as obtained by using dimensional analysis for a geometrically similar indenter.[39] As determined by the intercept between the curve and log F, different values of K_m are obtained for all the ECAE-deformed Al and the annealed Al. This suggests that under the present testing condition, the microstructure that developed from the ECAE process influenced the K_m value, while it had no effect on the constant n. The highest K_m is obtained for specimen B, which corresponds to the most severe plastic deformation. The K_m values for the ECAE specimens B and C are higher than those for the annealed and the specimen A.

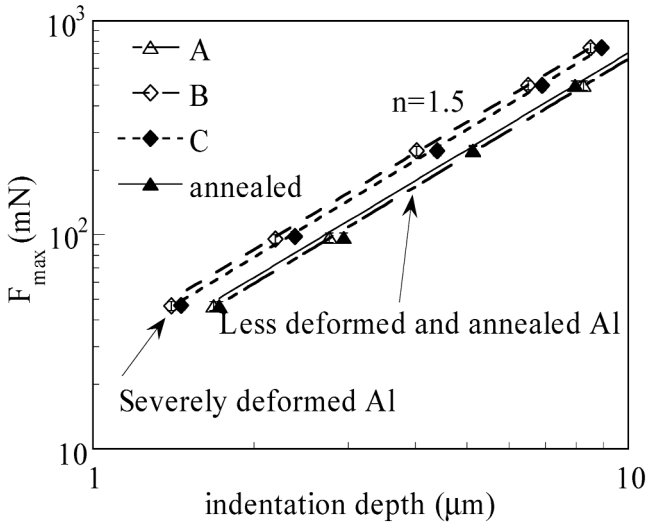

Fig. 3—Dependence of the indentation load on the maximum indentation depth (Δ: sample A, ◇: sample B, ◆: sample C, and ▲: annealed sample).

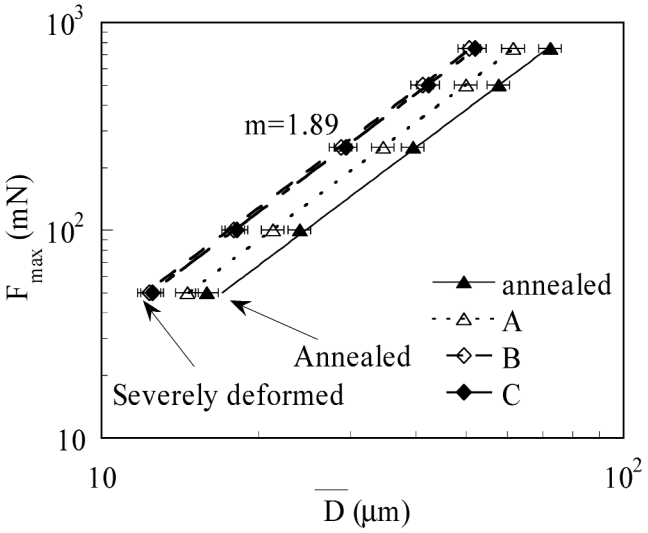

Fig. 4—Dependence of the indentation size on the indentation load (Δ: sample A, ◇: sample B, ◆: sample C, and ▲: annealed sample).

Both specimens B and C experienced severe plastic deformation, which resulted in higher dislocation densities that induced strong interaction between dislocations. Accordingly, K_m is more or less structure dependent.

B. *Microhardness and Residual Indentation Depth*

The indentation morphology was imaged on an optical microscope, from which both diagonals of the impression were measured and used to calculate the microhardness. For the same indentation load, a total of six indentations (note: two indentations in each specimen and three different specimens, A, B, and C, were prepared from three extruded Al rods) were performed to determine the average Vickers hardness.

The Meyer line is defined by a linear relation of[40,41]

$$\log F = m \log \overline{D} + \log a \qquad [16]$$

where $\overline{D}$ is the average length of the indentation diagonal; m is the Meyer index, which is characteristic of the material; and a is a constant. Figure 4 shows the Meyer lines for the indentations at the central location m for the ECAE-deformed samples (A, B, and C) and the annealed sample. A Meyer index of 1.89 is obtained for all samples. The largest indentation was made on the annealed sample, while samples B and C showed smaller resultant indentation sizes.

Using the measured diagonal lengths, one can calculate the apparent microhardness H_v by using Eq. [1], which did not account for the effect of pileup. The variation in the microhardness with the indentation load for both the ECAE-deformed Al and the annealed Al is shown in Figure 5. It is noted that the microhardness for both the ECAE-deformed and the annealed Al decreases with increasing indentation load, exhibiting the normal indentation size effect (ISE).[42,43,44] At the lowest indentation load of 50 mN, the microhardness of the ECAE-deformed samples B and C reaches a value of 0.6 GPa, whereas that of the annealed Al rises to about 0.37 GPa at the lowest load. The microhardness of sample A is about 0.45 GPa with an indentation load of 50 mN, which is slightly higher than that obtained

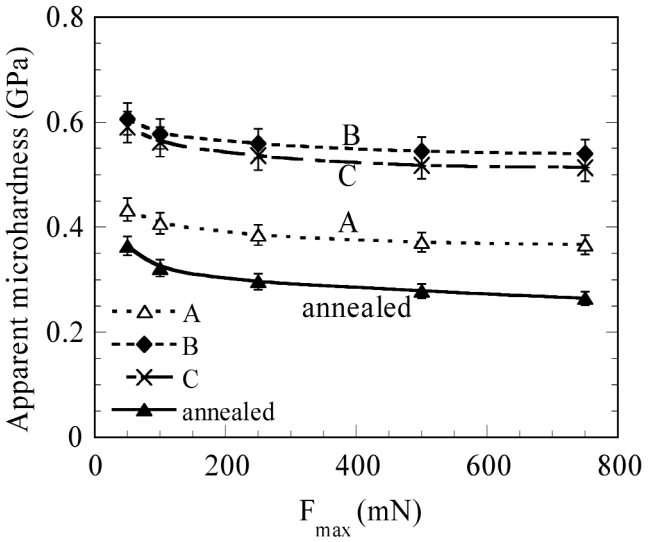

Fig. 5—Dependence of the apparent microhardness on the indentation load (Δ: sample A, ◇: sample B, ◆: sample C, and ▲: annealed sample).

in the annealed Al. Such a difference is due to the plastic deformation that occurred in specimen A during the ECAE process. This was introduced by the propagation of the deformation band at the bend of the material. The results suggest that the severe plastic deformation created during the passage through the sharp corner during the ECAE process led to microstructural change and resultant higher microhardness. One important observation is the softening in sample C compared to sample B, as indicated in Figures 3 through 5. Plastic recovery occurred once the material passed through the sharp corner; and dislocation annihilation processes occurred as a result of adiabatic heating.

Figure 6 shows the dependence of the residual indentation depth on the indentation load. It increases with the increasing indentation load, which induces more plastic deformation. The deepest residual indentation depth is observed in the annealed specimen, while the shallowest depth is

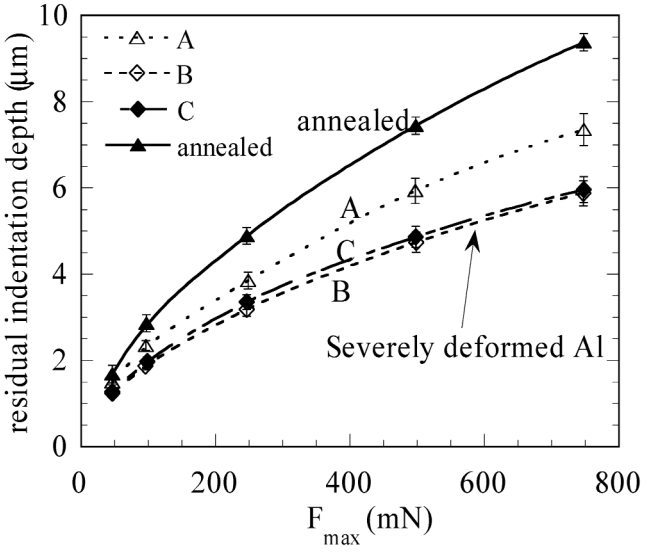

Fig. 6—Effect of the indentation load on the residual depth (Δ: sample A, ◇: sample B, ◆: sample C, and ▲: annealed sample).

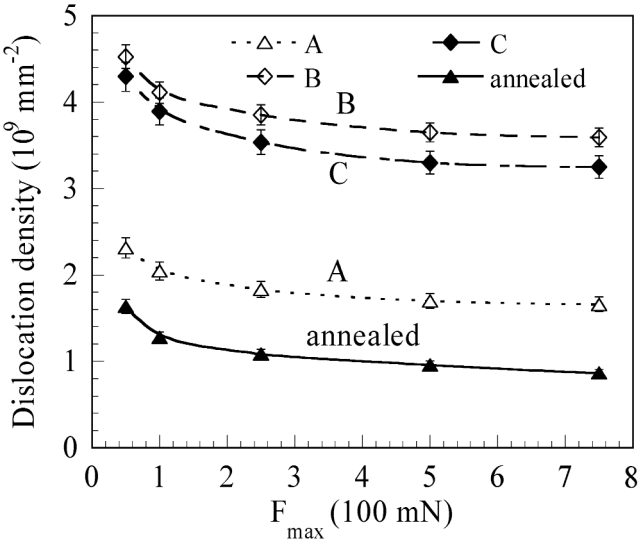

Fig. 7—Dependence of the dislocation density on the indentation load (Δ: sample A, ◇: sample B, ◆: sample C, and ▲: annealed sample).

observed in the ECAE-processed specimen B. This is in agreement with the dependence of the microhardness on the indentation location (Figure 5).

C. *Dislocation Density and Energy Dissipation*

Using $G = 26.1$ GPa for the shear modulus,[31] $\alpha = 0.3$ and $M = 1$ in Eqs. [1] and [6], the average dislocation density underneath the indentation is computed from Eq. [6]. The relation between the average dislocation density and the indentation load is depicted in Figure 7. It should be noted that the average dislocation density calculated from the microhardness includes the contribution of the dislocations previously stored in the sample and those generated during the indentation. The average dislocation density decreases with increasing indentation load. Specimens B and C have the highest dislocation densities due to severe plastic deformation created in the ECAE process, while the annealed Al exhibits the lowest dislocation density, as expected. The variation of the dislocation density as a function of the indentation load depends on the growth of the plastic zone underneath the indenter. As indicated in Eq. [8], the plastic zone increases with the indentation load and decreases with the dislocation density. Thus, the largest plastic size is produced in the annealed Al, which is in agreement with the results shown in Figure 6. Even though more dislocations were generated during indentation, the specific growth rate of the plastic zone ($c^{-1}\, dc/dt$) at a small indentation load was higher than the specific multiplication rate of dislocations ($\rho^{-1}\, d\rho/dt$). This led to a decrease in the average dislocation density. Once the specific multiplication rate of dislocations became comparable to the specific growth rate of the plastic zone, the average dislocation density approached an equilibrium value, as shown in Figure 6.

The energy dissipated in a loading-unloading cycle is plotted in Figure 8, where it is seen that less energy is dissipated in the ECAE-deformed Al compared to the annealed Al. This may be due to the higher dislocation density created in the ECAE process, which then increases the interaction of dislocations in the deformation zone. As expected, a larger indentation load creates more plastic deformation, which is associated with the multiplication and motion of dislocations. Accordingly higher plastic energy dissipation is observed for the annealed Al and specimen A.

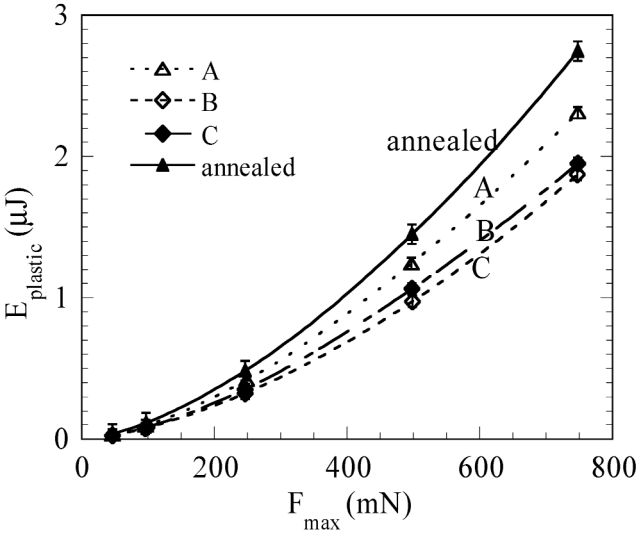

Fig. 8—Plastic energy dissipated in the indentations (Δ: sample A, ◇: sample B, ◆: sample C, and ▲: annealed sample).

The indentation-induced plastic deformation of the ECAE-deformed Al can be considered as consisting of two stages. In the first stage, dislocation multiplication occurs at the indenter tip, and the radii and numbers of these dislocation loops are enlarged with the increasing indentation depth. In the second stage, resistance to the movement of dislocation loops begins as a result of the dislocation substructure in the ECAE-deformed samples. Due to the interaction between dislocations, sufficiently high shear stress is required to cause the dislocation loops to grow in size and glide.

As shown in Eq. [14], the energy dissipated in the loading-unloading process is a function of the indentation load and

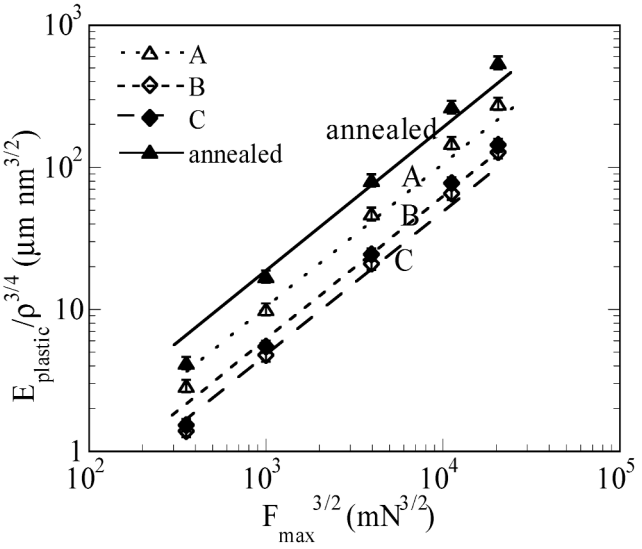

Fig. 9—Dependence of the plastic energy on the indentation load and local dislocation density (Δ: sample A, ◇: sample B, ◆: sample C, and ▲: annealed sample).

the dislocation density underneath the indenter. Figure 9 shows the relation between the energy dissipated divided by the dislocation density and the indentation load. Straight lines are fitted with the same slope through the data points for various samples. The experimental results support the proposed model.

V. SUMMARY

Based on the loading-unloading curves, the deformation behavior of the ECAE-deformed Al was discussed. A simple indentation model was proposed and the evolution of the dislocation density underneath the indentation was derived. The plastic energy dissipated in the loading-unloading process was found to be proportional to the 3/2 power of the indentation load and the 3/4 power of the dislocation density, which was supported by the experimental results.

The ECAE process introduced varying degrees of plastic deformation in the deformed Al rod, from which a variation of the microhardness with the various sections of the ECAE-deformed Al was observed. The hardness of the most severely deformed sample showed the highest hardness, as expected, and the annealed sample showed the lowest hardness, as expected. Independent of the microstructure, the normal indentation size effect was observed in both the ECAE-deformed Al and the annealed Al due to the competition between the nucleation of dislocations and the growth of plastic zone. During the unloading in the indentation of the ECAE-deformed Al, plastic recovery was observed, which suggested that a kind of Bauschinger effect occurred in the ECAE samples.

ACKNOWLEDGMENTS

This research is supported by the NSF through Grant No. DMR-0211706, monitored by Drs. Guebre Tessema and Bruce A. MacDonald, and the Kentucky Science and Engineering Foundation through Grant No. KSEF-148-502-03-73. The valuable comments by the reviewers are especially appreciated.

REFERENCES

1. J.S. Hayes, R. Keyte, and PB. Prangnel: *Mater. Sci. Technol.,* 2000, vol. 16, pp. 1259-63.
2. V.M. Segal, V.I. Reznikov, A.E. Drobyshevskiy, and V.I. Kopylov: *Russ. Metall.,* 1981, vol. 1, pp. 99-105.
3. V.M. Segal: *Mater. Sci. Eng.,* 1995, vol. A197, pp. 157-64.
4. Y. Iwahashi, Z. Horita, M. Nemoto, and T.G. Langdon: *Acta Mater.,* 1997, vol. 45, pp. 4733-41.
5. M. Furukawa, Z. Horita, M. Nemoto, and T.G. Langdon: *J. Mater. Sci.,* 2001, vol. 36, pp. 2835-43.
6. K. Matsubara, Y. Miyahara, Z. Horita, and T.G. Langdon: *Acta Mater.,* 2003, vol. 51, pp. 3073-84.
7. N.A. Smirnova, V.I. Levit, V.I. Pilyugin, R.I. Kuznetsov, L.S. Davydova, and V.A. Sazonova: *Fiz. Met. Metalloved.,* 1986, vol. 61, pp. 1170-77.
8. K. Nakashima, Z. Horita, M. Nemoto, and T.G. Langdon: *Mater. Sci. Eng.,* 2000, vol. A281, pp. 82-87.
9. R.Z. Valiev, D.A. Salimonenko, N.K. Tsenev, P.B. Berbon, and T.G. Langdon: *Scripta Mater.,* 1997, vol. 37, 1945-50.
10. Z. Horita, M. Furukawa, M. Nemoto, A.J. Barnes, and T.G. Langdon: *Acta Mater.,* 2000, vol. 48, pp. 3633-40.
11. H. Akamatsu, T. Fujinami, Z. Horita, and T.G. Langdon: *Scripta Mater.,* 2001, vol. 44, pp. 759-64.
12. Q. Wei, T. Jiao, S.N. Mathaudhu, E. Ma, H.T. Hartwig, and K.T. Ramesh: *Mater. Sci. Eng.,* 2003, vol. A358, pp. 266-72.
13. L. Cisar, Y. Yoshida, S. Kamado, Y. Kojima, and F. Watanabe: *Mater. Trans.,* 2003, vol. 44, pp. 476-83.
14. Z.A. Khan, U. Chakkingal, and P. Venugopal: *J. Mater. Process Technol.,* 2003, vol. 135, pp. 59-67.
15. H.Z. Ding, H. Mughrabi, and H.W. Hoppel: *Fatigue Fract. Eng. Mater.,* 2002, vol. 25, pp. 975-84.
16. A. Vinogradov and S. Hashimoto: *Adv. Eng. Mater.,* 2003, vol. 5, pp. 351-58.
17. S. Kokubo: *Sci. Rep. Tohoku Imperial Univ.,* 1932, vol. 21, pp. 256-62.
18. G. Sines and R. Carlson: *ASTM Bull.,* 1952, vol. 180, pp. 35-40.
19. G.U. Oppel: *Exp. Mech.,* 1964, vol. 21, pp. 135-40.
20. T.R. Simes, S.G. Mellor, and D.A. Hills: *J. Strain Analysis,* 1984, vol. 19, pp. 135-37.
21. J.G. Swadener, B. Taljat, and G.M. Pharr: *J. Mater. Res.,* 2001, vol. 16, pp. 2091-102.
22. H. Widersich: *J. Met.,* 1963, vol. 15, pp. 423-28.
23. H. Conrad, K. Okazoki, V. Gadgil, and M. Jon: *Electron Microscopy and Strength of Materials,* University of California Press, Berkeley, CA, 1972, pp. 453-55.
24. F.R.N. Nabarro, Z.S. Basinski, and D.B. Holt: *Adv. Phys.,* 1964, vol. 13, pp. 193-250.
25. M.E. Kassner: *J. Mater. Sci.,* 1990, vol. 25, pp. 1997-2003.
26. R.L. Jones and H. Conrad: *TMS-AIME,* 1969, vol. 245, pp. 779-84.
27. J.E. Bailey and P.B. Hirsch: *Phil. Mag.,* 1960, vol. 5, pp. 485-90.
28. G.I. Taylor: *Proc. R. Soc.,* 1934, vol. A145, pp. 362-70.
29. M.F. Ashby: *Phil. Mag.,* 1970, vol. 21, pp. 399-405.
30. M.E. Kassner: *Acta Mater.,* 2004, vol. 52, pp. 1-9.
31. M.A. Meyers and K. Kumarchawla: *Mechanical Behavior of Materials,* Prentice-Hall, Inc., Upper Saddle River, NJ, 1998.
32. D.M. Marsh: *Proc. R. Soc.,* 1964, vol. A279, pp. 420-30.
33. R. Hill: *The Mathematical Theory of Plasticity,* Clarendon Press, Oxford, UK, 1950.
34. K.L. Johnson: *Contact Mechanics,* Cambridge University Press, New York, NY, 1987.
35. H. Mecking: in *Work Hardening in Tension and Fatigue,* A.W. Thompson, ed., TMS, Warrendale, PA, 1977, p. 67.
36. L.L. Peng, F.Q. Yang, and K. Okazaki: *in Ultrafine Grained Materials III,* Y.T. Zhu, T.G. Langdon, R.Z. Valiev, S.L. Semiatin, D.H. Shin, and T.C. Lowe, eds., TMS, Warrendale, PA, 2004, pp. 535-41.
37. K. Tanaka: *J. Mater. Sci.,* 1987, vol. 22, pp. 1501-10.
38. J.L. Hay, W.C. Oliver, A. Bolshakov, and G.M. Pharr: *Mater. Res. Soc. Symp. Proc.,* 1998, vol. 522, pp. 101-06.
39. Y.T. Cheng and C.M. Cheng: *Int. J. Solids Struct.,* 1999, vol. 36, pp. 1231-43.
40. G.E. Dieter: *Mechanical Metallurgy,* 2nd ed., McGraw-Hill, Inc., New York, NY, 1976, p. 392.
41. J.S. Field and M.V. Swain: *J. Mater. Res.,* 1993, vol. 8, pp. 297-306.
42. F.Q. Yang, J.Y.Y. Zhou, V. Kordonski, and S.D. Jacobs: *J. Mater. Sci. Lett.,* 1996, vol. 15, pp. 1523-25.
43. W.D. Nix and H.J. Gao: *J. Mech. Phys. Solids,* 1998, vol. 46, pp. 411-25.
44. R. Rodriguez and I. Gutierrez: *Mater. Sci. Eng.,* 2003, vol. A361, pp. 377-84.